Influence of the geometric parameters of a vertical rotational single-sheet tester on sample field homogeneity

Guilherme Costa Ayres Tolentino, Guillaume Parent, Olivier Ninet, Mathieu Rossi, Jean Vianei Leite, Jonathan Blaszkowski

Influence of the Geometric Parameters of a Vertical Rotational Single Sheet Tester on Sample Field Homogeneity

Guilherme C. A. Tolentino
Univ. Artois, UR 4025
Laboratoire Systèmes Électrotechniques et Environnement (LSEE)
F-62400 Béthune, France
Guillaume Parent *Univ. Artois, UR 4025*
Laboratoire Systèmes Électrotechniques et Environnement (LSEE)
F-62400 Béthune, France
Olivier Ninet *Univ. Artois, UR 4025*
Laboratoire Systèmes Électrotechniques et Environnement (LSEE)
F-62400 Béthune, France
Mathieu Rossi *Univ. Artois, UR 4025*
Laboratoire Systèmes Électrotechniques et Environnement (LSEE)
F-62400 Béthune, France
Jean Vianei Leite
Universidade Federal de Santa Catarina, GRUCAD
Santa Catarina, Florianòpolis, Brazil
Jonathan Blaszkowski
Thyssenkrupp Electrical Steel, F-62330 Isbergues, France

Abstract

Purpose - The horizontal Rotational Single Sheet Tester (RSST) suffers from weaknesses such as the reduced size of test samples, measurement disturbances due to magnetic flux leakage and non-homogeneity of field in the measurement area. Although the vertical RSST allows to overcome the first two aforementioned drawbacks, the heterogeneity of the field in the test sample remains an issue. Additionally, there is still a lack of device standardization to ensure test repeatability, as already is well established with the Epstein frame. The aim of this paper is to investigate the influence of several parameters on the field homogeneity in the test sample.

Design/methodology/approach - A fully 3D finite element model of a vertical RSST is developed and used to perform a sensibility study on several geometrical parameters.

Findings - The influence of several parameters on the field homogeneity in the test sample, such as the geometrical dimensions of the yokes, the presence or not of holes drilled inside the test sample for B-coil placement as well as the size of the H-coils and B-coils are addressed.
Originality/value - It is expected that this study will contribute to the optimization and standardization vertical RSSTs.
Keywords - RSST ; Magnetic Characterization Device ; Finite element analysis ; Magnetic field
Paper Type - Research paper

1 Introduction

Nowadays, the design of an electrical machine – whether it is a transformer or a rotating machine – can be achieved my means of several methods such as analytical methods, lumped parameter equivalent circuit, finite element method, etc. Whatever method is involved, one of the Achilles heel lies in the behavioral model that is used to represent the constitutive equations, in particular the relation between the magnetic field **H** and the magnetic flux density **B**. Several behavioral models are reported in the literature, each one allowing to take into account, or not, different kind of phenomena, such as non linearity, hysteresis, rotational magnetization, anisotropy, etc (Tumanski, 2011). In fact, when it comes to designing an electrical machine, using a behavioral model accounting for rotational magnetization and/or anisotropy can be a key point, and such a model has to be built on relevant measurements made with a two-dimensional characterization device (Tumanski, 2011; Sievert, 2011).

From the 80s, numerous works have been done on the subject, and several two-dimensional characterization devices can be found in the literature (de la Barriere et al., 2018), each one having its pros and cons. An unfortunate consequence of that large variety of devices, in terms of topologies and geometries, is that it is difficult to set a standard, such as those that exist for the Single Sheet Tester (SST) (IEC, 1992) or the Epstein Frame (IEC, 2008).

The horizontal Rotational Sheet Tester (RSST), originally introduced in (Brix, 1982; Brix et al., 1982), has been widely studied since then (Enokizono et al., 1990; Zhu and Ramsden, 1993; Salz, 1994; Hasenzagl et al., 1996; Makaveev et al., 2000; Sievert et al., 2007; Maeda et al., 2008). It suffers from three main issued. Firstly, the small size of the test sample, which is an issue in case of grain oriented electrical steel sheet with large grains. Secondly, the flux leakage between the adjacent salient poles, as reported in (Makaveev et al., 2000). Thirdly, the high non-homogeneity of both **H** and **B** (Tumanski, 2005; Leite et al., 2007).

Another approach allowing to overcome this drawback consists in considering a topology similar to a conventional three-phase induction machine, the rotor being simply replaced by a round-shape test sample (Wanjiku and Pillay, 2015; Wanjiku and Pillay, 2016; Akiror et al., 2018). A variant of this topology consists in magnetizing the same kind of round-shape test sample by a system of electromagnets working as a Halbach array of magnets (Wanjiku and Pillay, 2015; Wanjiku and Pillay, 2016; Yue et al., 2019b). Nevertheless, in both cases the homogeneity remains an issue.

The vertical RSST has been introduced in the early 90s (Sievert et al., 1992; Zouzou et al., 1992; Enokizono et al., 1992) but is still under consideration in recent publications (Fonteyn and Belahcen, 2008; Li et al., 2017; Yue et al., 2019b; Yue et al., 2019a). It derives from the standardized SST. According to the literature, the advantages of this setup are numerous. Firstly, its ease of implementation due to similarities to the standardized SST. Secondly, a better homogeneity of $\mathbf{H}$ and $\mathbf{B}$ in the middle of the test sample (de la Barriere et al., 2018). Thirdly, it allows to reach higher flux density levels in the test sample than the horizontal SST (Fonteyn and Belahcen, 2008; Miyagi et al., 2009). It has to be noted that each publication related to that device brings its own setup in terms of numbers and dimensions of the yokes as well as on dimensions of sensors (Nencib et al., 1994; Nencib et al., 1995; Nencib et al., 1996b; Nencib et al., 1996a; Dalton et al., 1996; Tumanski and Bakon, 2001). Nevertheless, the trend emerging from all those publications is that the larger the yokes width, the better. Indeed, in (De Wulf et al., 2003) the authors evaluate the accuracy of miniature SSTs dedicated to the characterization of small size test samples and highlight a difference with the results obtained using an Epstein frame that can be up to 5 %. The same trend is highlighted on vertical RSSTs in (Nencib et al., 1994; Nencib et al., 1995; Nencib et al., 1996b). Moreover, larger yokes allow to properly characterize larger test samples (Sievert et al., 1992), the latters allowing to "eliminate the influence of the demagnetizing field" (Tumanski, 2011). However, the standards relative to the regular SST (IEC, 1992; IEC, 2018) allow the use of yokes of any size "as long as the relevance of the results is ensured". To the authors' knowledge, almost no quantitative study of the influence of those parameters in the homogeneity of the field seen by the sensors has been published except in (Nencib et al., 1994; Nencib et al., 1995; Nencib et al., 1996b) in which the focus is made on the deviation of the mean value in the very center of the sample only. Above all, in all of the aforementioned studies, no link is made between the non homogeneity of the fields in the sample and the actual value that would be measured with actual sensors, which is after all the most important when characterizing a material. In particular, none of those works takes into consideration that the sensors employed to evaluate $\mathbf{H}$ and $\mathbf{B}$ are not of the same dimensions nor do they account for the fact that the more often $\mathbf{B}$ is evaluated by means of a coil requiring to drill the test sample. Yet, there is no doubt those holes are of great influence.

This is the aim of this paper which is divided into four sections. In the first one, the studied device as well as the protocol are introduced. In the second section, the influence of the yokes' size on the homogeneity of both $\mathbf{H}$ and $\mathbf{B}$ in the sample is assessed. In the third section, the studied area are restricted to those that would be covered by actual sensors. Finally, the influence of drilled holes in the test sample is addressed in the fourth section.

2 Topology of the studied vertical RSST and finite element model

An overview of the topology of the studied vertical RSST is presented in Fig. 1a. It is composed of two magnetic yokes, i.e. one per phase. Each yoke consists

Table 1: Dimensions of the vertical RSST. *Source: authors own work*

Name	Value
W_s	300 mm
T_s	0.35 mm
W_yl	20 mm
W_y	290 mm
H_y	150 mm (Small core) or 200 mm (Tall core)
T_y	Varies between 75 mm and 200 mm
W_h	Varies between 20 mm and 50 mm
W_b	Varies between 20 mm and 50 mm
D_b	1 mm

of two C-shape cores (see Fig. 1b) arranged along each side of the test sample. Due to geometrical constraints and for the sake of magnetic balance between the two yokes, the two cores share every dimensions W_yl, W_y and T_y but the height H_y (see Fig. 1a). The test sample is square with side and thickness denoted W_s and T_s respectively. The layout of the sensors is presented in Fig. 1c. The H-coil is square-shaped with a size denoted W_h and is placed in the middle of the test sample. Holes of diameter denoted D_b are drilled in the test sample in order to place the B-coil. The latter has a thickness equal to D_b and its width is denoted W_b. All dimensions are summarized in table 1.

The finite element simulations are conducted using the softwares GMSH (Geuzaine and Remacle, 2009) and GetDP (Dular et al., 1998). The model is fully 3D which leads to meshes made of an important number of tetraedra. As examples, the smallest (cases where $T_\mathrm{y} = 75\,\mathrm{mm}$) and biggest (cases where $T_\mathrm{y} = 200\,\mathrm{mm}$) meshes are made of 265 000 and 632 000 tetraedra respectively. Please note that emphasis is put on the test sample, which is meshed with three layers of elements in its thickness. As for the resolution of the problem, the magnetostatic scalar potential formulation is used instead of the vector potential formulation for time computation reduction. The yokes are considered to have a linear behavior with a relative permeability equal to 10 000. Moreover, the nonlinear behavior of the test sample is taken into account by means of its first magnetization curve. In the following, the test sample is made of M260 electrical steel whose first magnetization curve is presented in Fig. 3. Finally, for the sake of both clarity and relevance of the analysis, only the worst case in terms of field homogeneity in the test sample, that is the case in which the latter is magnetically excited along its diagonal, is considered and presented.

3 Field homogeneity inside the test sample

3.1 Context

In this section, no sensor is considered and the holes (see Fig. 1c) are not taken into account in the simulation model either. Let $\|\mathbf{H}_\mathrm{center}\|$ and $\|\mathbf{B}_\mathrm{center}\|$ be the values of $\mathbf{H}$ and $\mathbf{B}$ respectively at the very center of the test sample. As an illustration, Fig. 2 shows distribution maps of $\mathbf{H}$ and $\mathbf{B}$ inside the test sample for $\|\mathbf{B}_\mathrm{center}\| = 0.75\,\mathrm{T}$ $\|\mathbf{B}_\mathrm{center}\| = 1.55\,\mathrm{T}$ with $T_\mathrm{y} = 200\,\mathrm{mm}$. One can easily ob-

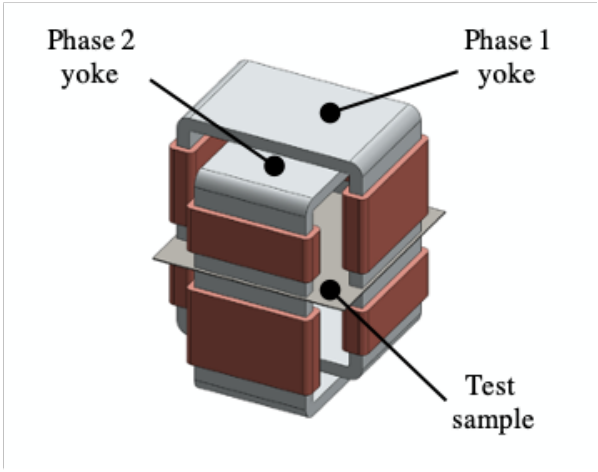

(a) Topology of the studied vertical RSST

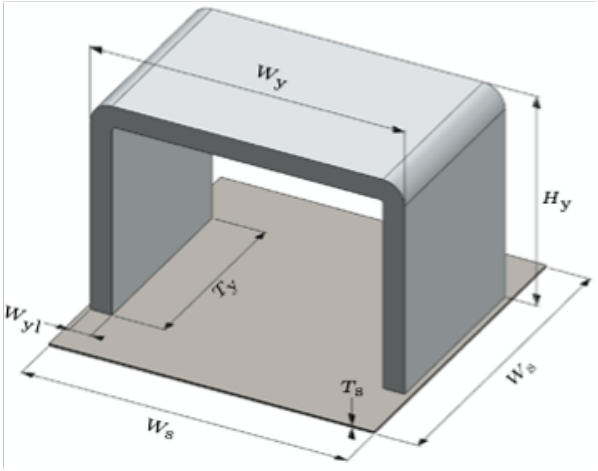

(b) Dimensions of the test sample and a half of a yoke

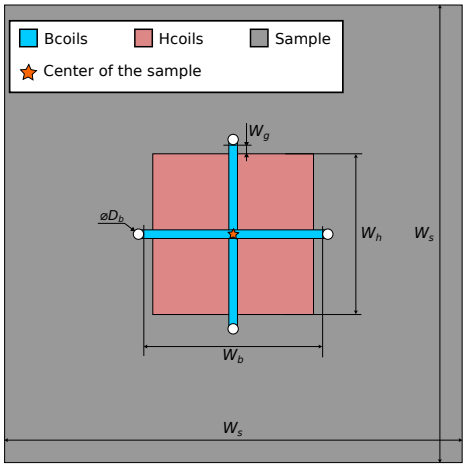

(c) Layout of the H-coils and B-coils

Figure 1: Studied vertical RSST. *Source: authors own work*

serve that they are widely inhomogeneous. To take the analysis a step further, Fig. 3 shows the values of both $\mathbf{H}$ and $\mathbf{B}$ occurring in different areas of the test sample for different levels of magnetization, still with $T_\mathrm{y} = 200\,\mathrm{mm}$. The first magnetization curve of the M260 electrical steel is also shown, in black, for information purpose. It can immediately be noted in this figure that both $\mathbf{H}$ and $\mathbf{B}$ inside the whole test sample, shown in blue, are widely heterogeneous due to its large size as well as due to the topology of the RSST. Indeed, whatever the excitation value, very low magnetic flux occurs in the corner regions of the sample. However, high magnetic flux values occur at the junction between the cores and the test sample. One might consider that this is not so much an issue since an actual sensor would only cover a small area (a few cm^2) of the test sample. As an illustration, the red marks in Fig. 3 show the values of $\mathbf{H}$ and $\mathbf{B}$ occurring in a square area with a size of 50 mm located at the center of the test sample. As expected, the field distribution inside this area is way more homogeneous. Nevertheless, Fig. 3 clearly highlights that even inside such a limited area the heterogeneity is still noticeable. Moreover, the mean values of $\mathbf{H}$ and $\mathbf{B}$, which correspond to the values that would be given by an actual square-shaped sensor of 50 mm of side, do not match $\|\mathbf{H}_\mathrm{center}\|$ and $\|\mathbf{B}_\mathrm{center}\|$. This will be addressed in Section 4.

3.2 Influence of the core length T_y

In order to study the influence of T_y on the homogeneity of $\mathbf{H}$ and $\mathbf{B}$, let's still consider a square area with a size of 50 mm (i.e. $W_\mathrm{h} = W_\mathrm{b} = 50\,\mathrm{mm}$) located at the center of the test sample. The values of $\mathbf{H}$ and $\mathbf{B}$ inside this area with respect to T_y are represented as box and whisker plots in Fig. 4. T_y varies from 75 mm to 200 mm in increments of 25 mm and three different magnetization levels at the very center of the test sample are studied: $\|\mathbf{B}_\mathrm{center}\| \in \{0.35\,\mathrm{T}; 0.75\,\mathrm{T}; 1.55\,\mathrm{T}\}$. Those three values are chosen for their relevance: $\|\mathbf{B}_\mathrm{center}\| = 0.35\,\mathrm{T}$ corresponds to a low magnetization level, i.e. the beginning of the linear part of the first magnetization curve, $\|\mathbf{B}_\mathrm{center}\| = 0.75\,\mathrm{T}$ corresponds to the middle of the linear part of the first magnetization curve, and $\|\mathbf{B}_\mathrm{center}\| = 1.55\,\mathrm{T}$ corresponds to the post knee area (see Fig. 3).

The first conclusion that can be drawn from Fig. 4 is that no matter the value of T_y nor the value of the magnetization level, outliers are always present. There is no doubt those outliers have an influence on the value given by actual sensors. The second conclusion is that the homogeneity of both $\mathbf{H}$ and $\mathbf{B}$ increases with T_y, even if it may be noted that as soon as T_y is superior to half the width of the test sample the results are much the same.

In view of these results, it appears that the relevance of measurements made on this kind of RSST will be greatly improved by using the largest core length T_y possible.

4 Fields Seen by actual H-coils and B-coils

As mentioned in section 3.1, the homogeneity inside a small square-shaped area located at the middle of the test sample, which corresponds to the area covered by a typical H-coil (see Fig. 1c), can be suitable. However, a B-coil is not square-shaped. Then, in the present section, we focus on the distribution of $\mathbf{H}$

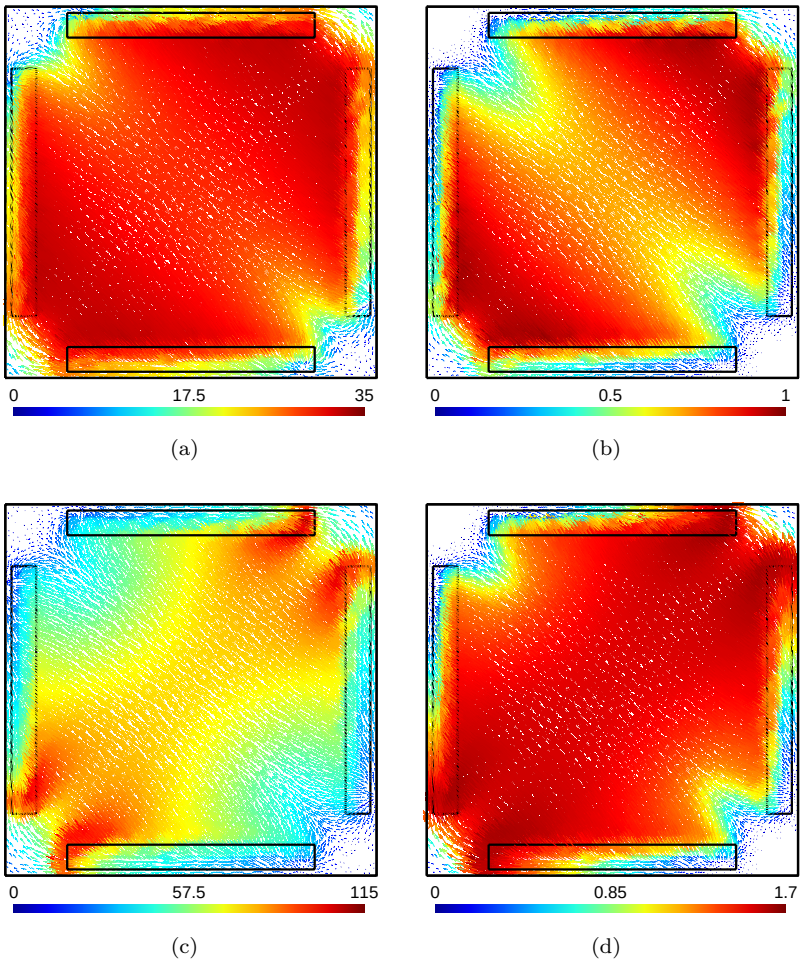

Figure 2: Distribution of $\mathbf{H}$ (*left*) and $\mathbf{B}$ (*right*) inside the test sample for $\|\mathbf{B}_{\text{center}}\| = 0.75\,\text{T}$ (*top*) and $\|\mathbf{B}_{\text{center}}\| = 1.55\,\text{T}$ (*bottom*). *Source: authors own work*

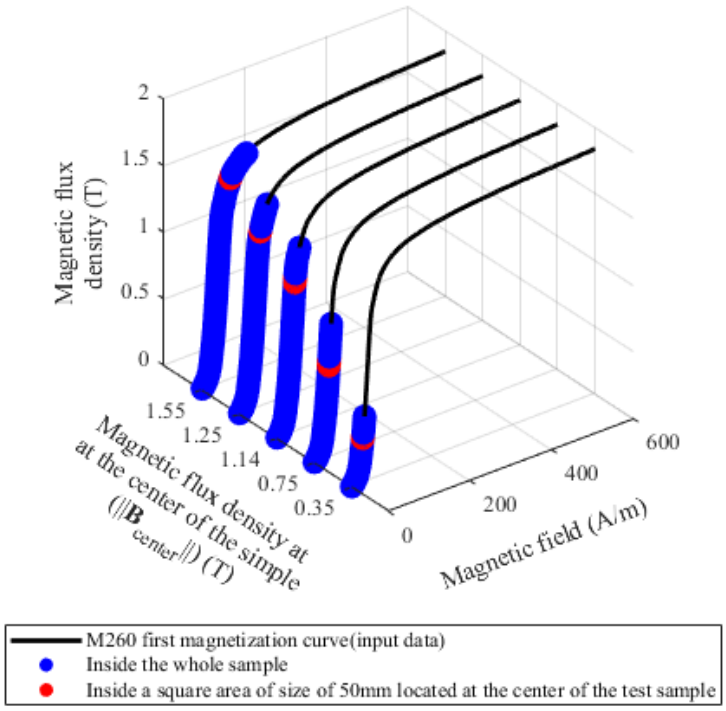

Figure 3: Distribution of $\mathbf{H}$ and $\mathbf{B}$ inside different areas of the test sample for several values of $\|\mathbf{B}_{\text{center}}\|$ and with $T_{\text{y}} = 200\,\text{mm}$. *Source: authors own work*

and $\mathbf{B}$ seen by H-coils and B-coils such as the ones presented in Fig. 1c. Please note that in this section the holes (see Fig. 1c) are still not taken into account in the simulation model. Three dimensions of sensors are addressed: $W_{\text{h}} \in \{20\,\text{mm}; 35\,\text{mm}; 50\,\text{mm}\}$ and $W_{\text{b}} = W_{\text{h}}$.

Let $\langle\|\mathbf{H}_{\text{H-coil}}\|\rangle$ and $\langle\|\mathbf{B}_{\text{B-coil}}\|\rangle$ be the mean values of $\mathbf{H}$ and $\mathbf{B}$ seen by the H-coils and the B-coils respectively. As previously mentioned, $\langle\|\mathbf{H}_{\text{H-coil}}\|\rangle$ and $\langle\|\mathbf{B}_{\text{B-coil}}\|\rangle$ represent the values that would be given by actual sensors. In order to study the influence of the field heterogeneity on those values, they are compared to $\|\mathbf{H}_{\text{center}}\|$ and $\|\mathbf{B}_{\text{center}}\|$ respectively. The variation of the relative error $\epsilon_{\text{X}} = 100\left|\frac{\langle\|\mathbf{X}_{\text{X-coil}}\|\rangle - \|\mathbf{X}_{\text{center}}\|}{\|\mathbf{X}_{\text{center}}\|}\right|$, where the subscript "X" is either "H" or "B", with respect to T_{y} is presented in Fig. 5.

It confirms that larger values of T_{y} lead to a higher homogeneity whatever the values of W_{h} and W_{b}. This clearly appears in Figs. 5a and 5b. Figure 5c, as for it, may suggest that $T_{\text{y}} = 125\,\text{mm}$ gives lower error values. However, the error values have to be considered globally, i.e. on the whole magnetization range. Actually, the maximum values of ϵ_{H} and ϵ_{B} are 0.66 % and 0.19 % for $T_{\text{y}} = 125\,\text{mm}$ whereas they are 0.54 % and 0.31 % for $T_{\text{y}} = 200\,\text{mm}$ (with $W_{\text{h}} = W_{\text{b}} = 50\,\text{mm}$). Figure 5 also highlights that small size of sensors leads to small values of the relative error, which was expected. However, the divergence of both ϵ_{H} and ϵ_{B} with W_{h} and W_{b} is very low (under 1 %) which means that sensors of a size of 50 mm can provide a relevant measurement. This is a main outcome for the vertical RSST compared to the horizontal RSST when it comes to characterize grain oriented electrical steel given that the size of a grain of

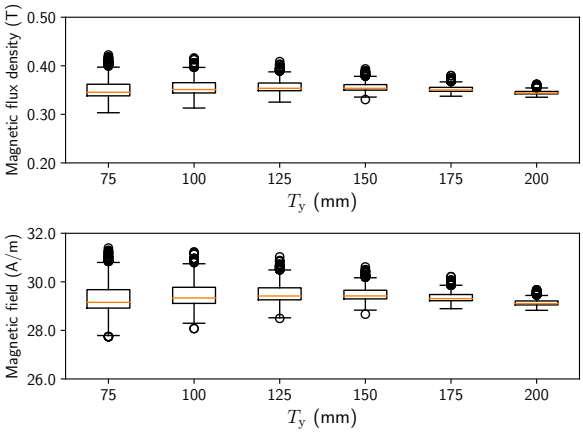

(a) $\|\mathbf{B}_{\text{center}}\| = 0.35\,\text{T}$ at the center of the test sample.

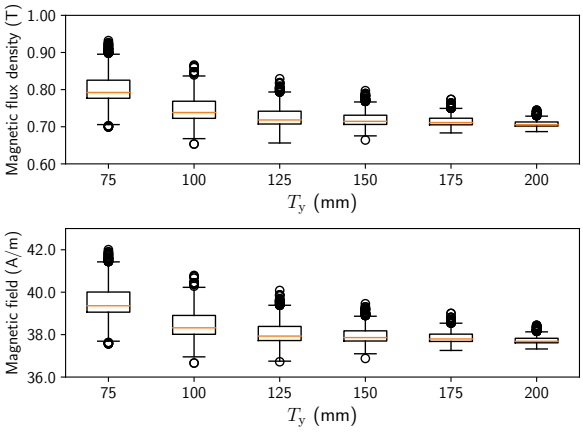

(b) $\|\mathbf{B}_{\text{center}}\| = 0.75\,\text{T}$ at the center of the test sample.

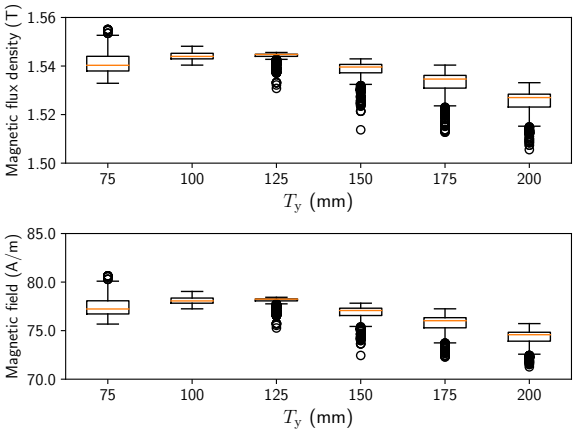

(c) $\|\mathbf{B}_{\text{center}}\| = 1.55\,\text{T}$ at the center of the test sample.

Figure 4: Values of $\|\mathbf{H}\|$ and $\|\mathbf{B}\|$ under the statistical box plot analysis, obtained by FEM simulation inside a square area of size of 50 mm located at the center of the test sample with respect to T_y for different values of $\|\mathbf{B}_{\text{center}}\|$. *Source: authors own work*

such a material can be up to a few cm (Qiu et al., 2017) and that a relevant measurement requires that the sensors cover between 4 and 6 grains (Walpole, 1985).

5 Influence of holes - Link to actual measurements

5.1 With B-coil and H-coil sharing the same width

The results shown in Fig. 5 lead to the conclusion that the size of the sensors does not significantly impact the relevance of the value of $\langle \|\mathbf{H}_{\text{H-coil}}\| \rangle$ and $\langle \|\mathbf{B}_{\text{B-coil}}\| \rangle$, and thus the relevance of the measured values. However, the holes drilled into the test sample for the placement of the B-coils were not taken into account. There is no doubt that the local saturations that will occur in their vicinity will impact the homogeneity of the fields seen by both the H-coils and the B-coils.

For the sake of relevance of the comparison, the conditions remain the same as in section 4, i.e. $W_{\text{h}} = W_{\text{b}}$, with addition of holes flush to the H-coil ($W_{\text{g}} = 0\,\text{mm}$) in the test sample (see Fig. 1c). Fig. 6 shows the variations of ϵ_{H} and ϵ_{B} in such conditions with respect to T_{y}. Two main conclusions can be drawn from the comparison between Figs. 5 and 6. Firstly, the holes have a non negligible impact on $\langle \|\mathbf{H}_{\text{H-coil}}\| \rangle$ and $\langle \|\mathbf{B}_{\text{B-coil}}\| \rangle$ since the values of ϵ_{H} and ϵ_{B} are now up to 3 % and 4 % respectively (see Fig. 6c). Secondly, using the largest sensors ($W_{\text{h}} = W_{\text{b}} = 50\,\text{mm}$) globally, i.e. over a wide magnetization level band, lead to the lowest values of ϵ_{H} and ϵ_{B}. These outcomes strengthens the conclusion drawn in section 4 about using large sensors.

5.2 Influence of the distance between the holes and the H-coil

The results previously presented highlighted the influence of the holes on the accuracy of the values provided by the sensors. Given that the local saturation appearing in the vicinity of holes are responsible for the increase of ϵ_{H} and ϵ_{B} and that in section 5.1 the H-coils are flush to the holes, this section focuses on the impact of W_{g} (see Fig. 1c).

The variation of ϵ_{H} with W_{g} is shown in Fig. 7. The conclusions that can be drawn are twofold. Firstly, the values provided by the two largest sensors are not impacted by W_{g}. Secondly, W_{g} has an impact when using a small sensor. As shown in Fig. 7a, it is possible to significantly reduce ϵ_{H} under 1 % by drastically increasing W_{g}. However, from a practical point of view, this is not a solution due to the difficulty of manufacturing and the very low signal level that such small size H-coils are able to generate.

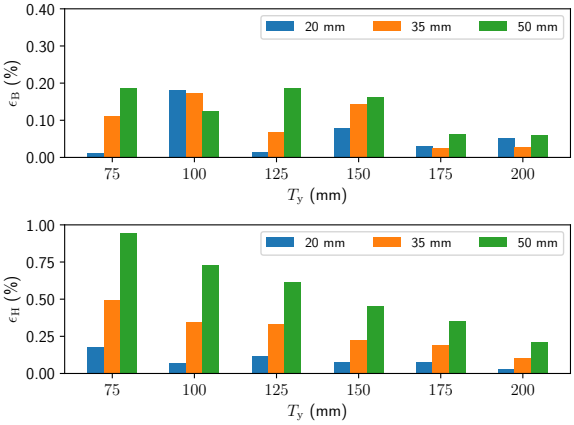

(a) $\|\mathbf{B}_{\text{center}}\| = 0.35\,\text{T}$.

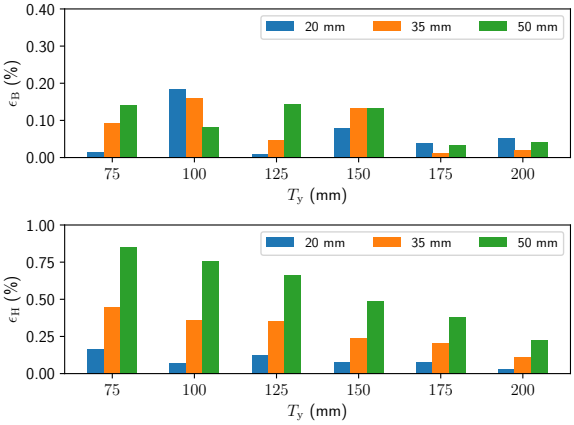

(b) $\|\mathbf{B}_{\text{center}}\| = 0.75\,\text{T}$.

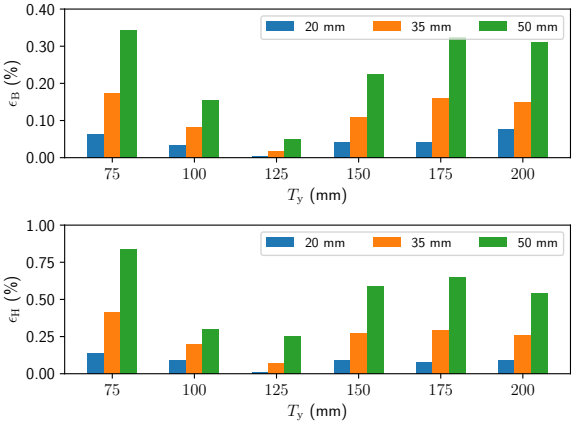

(c) $\|\mathbf{B}_{\text{center}}\| = 1.55\,\text{T}$.

Figure 5: Variation of ϵ_H and ϵ_B with respect to T_y when B-coils holes are not taken into account. *Source: authors own work*

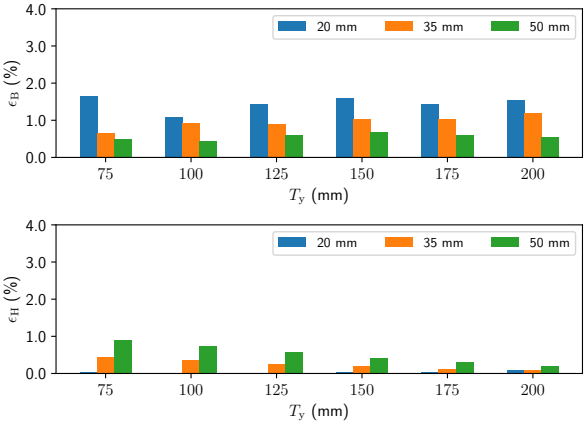

(a) $\|\mathbf{B}_{\text{center}}\| = 0.35\,\text{T}$.

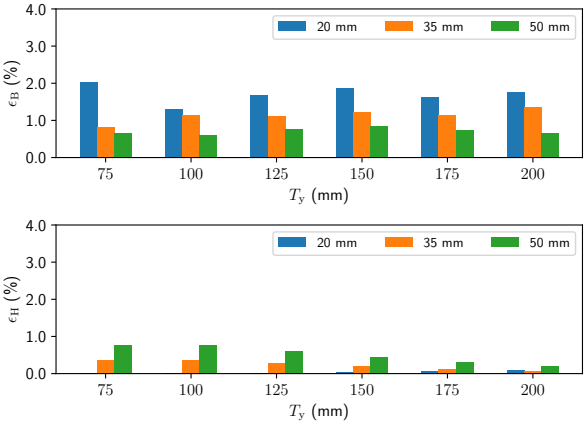

(b) $\|\mathbf{B}_{\text{center}}\| = 0.75\,\text{T}$.

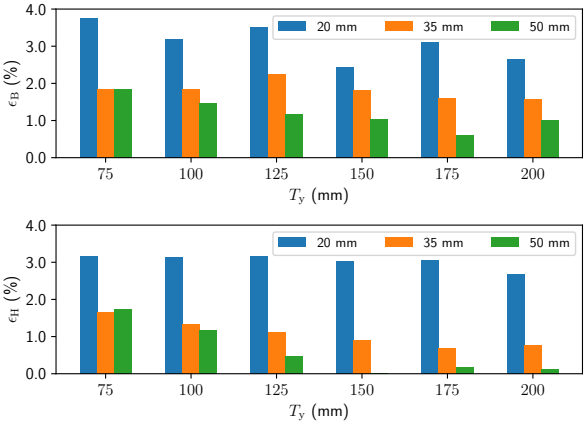

(c) $\|\mathbf{B}_{\text{center}}\| = 1.55\,\text{T}$.

Figure 6: Variation of ϵ_{H} and ϵ_{B} with respect to T_{y} when B-coils holes are taken into account ($W_{\text{h}} = W_{\text{b}}$). *Source: authors own work*

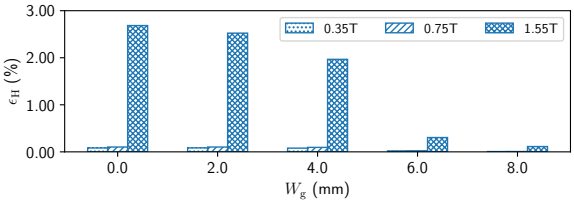

(a) $W_b = 20\,\text{mm}$

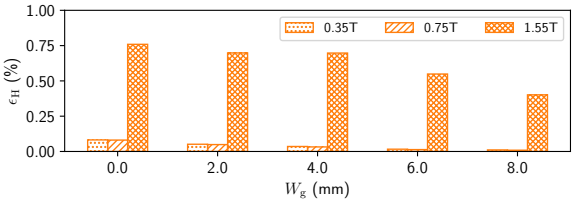

(b) $W_b = 35\,\text{mm}$

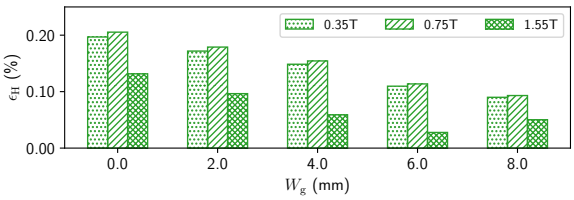

(c) $W_b = 50\,\text{mm}$

Figure 7: Variation of ϵ_H with respect to W_g ($T_y = 200\,\text{mm}$). *Source: authors own work*

6 Conclusion

The work presented in this paper highlights that the accuracy of the results given by a vertical RSST largely depends on several geometrical parameters, such as the width of the yokes used to magnetize the test sample, the dimensions of the sensors – H-coils and B-coils – as well as the presence of the holes required for the placement of the B-coils. The study is focused on the homogeneity of both the magnetic field and flux density seen by the sensors since they are of great influence on the values reported by them.

Firstly, the influence of the width of the yokes is addressed in section 3. On that topic, it is usually reported in the literature that "the larger the better". Nevertheless, the results presented in this section show that this conclusion is not entirely correct since no significant improvement can be seen regarding the homogeneity of the field seen by the sensors as soon as the width the the yokes is greater than half the width of the test sample. In practice, this allows for a reduction of the size – and thus the cost – of the RSST.

Secondly, the influence of the sensors size is addressed in section 4. Keeping in mind that the homogeneity of the fields seen by the sensors is a key point, it seems natural to choose them as small as possible. On that topic, it is reported in (Zurek, 2017) that the size of an H-coil depends on the zone of interest which is why even if a commonly used size for rotational measurements is around 20 mm × 20 mm some researchers use 50 mm × 50 mm sensors. The results presented in section 4 show that in the case when a non intrusive method, i.e. a method that does not require any drilled hole in the test sample such as the needle-based method (Tumanski, 2011), is used for the measurement of $\mathbf{B}$, the size of the sensors does not really matter. Then, the best option is to use a 50 mm × 50 mm H-coil, for two reasons. Firstly, it will allow for taking into account of more grains than smaller sensors. While this is not an issue in the case of test sample made of non oriented steel, it becomes a key point when it comes to deal with grain oriented steel since a relevant measurement requires that the sensors cover between 4 and 6 grains while the size of a grain of such a material can be up to a few cm. Secondly, a large H-coil allows for more turns which lead to higher output signals, and thus an easier signal conditioning.

Finally, the influence of the holes drilled in the test sample to place the B-coil is addressed in section 5. The results presented in this section show that the presence of holes can be an issue when using small sensors, but has no impact on the results provided by a 50 ×50 mm H-coil with a 50 mm B-coil, which support the choice of "big" sensors.

References

(1992). IEC60404: Magnetic materials - Part 3: Methods of measurement of the magnetic properties of magnetic sheet and strip by means of a single sheet tester. Technical report, International Electrotechnical Commission.

(2008). IEC60404: Magnetic alloys and steels - Part 2 - Methods of measurement of the magnetic properties of electrical steel strip and sheet by means of an Epstein frame. Standard, International Electrotechnical Commission.

(2018). IEC60404: Magnetic materials - Part 16: Methods of measurement of the magnetic properties of Fe-based amorphous strip by means of a single sheet tester. Technical report, International Electrotechnical Commission.

Akiror, J. C., Wanjiku, J., Pillay, P., Cave, J., and Merkhouf, A. (2018). Rotational Core Loss Magnetizer: Design and Measurements. *IEEE Transactions on Industry Applications*, 54(5):4355–4364. doi: 10.1109/TIA.2018.2844844.

Brix, W. (1982). Measurements of the rotational power loss in 3% silicon-iron at various frequencies using a torque magnetometer. *Journal of Magnetism and Magnetic Materials*, 26(1-3):193–195. doi: 10.1016/0304-8853(82)90151-2.

Brix, W., Hempel, K., and Schroeder, W. (1982). Method for the measurement of rotational power loss and related properties in electrical steel sheets;. *IEEE Transactions on Magnetics*, 18(6):1469–1471. doi: 10.1109/TMAG.1982.1062088.

Dalton, J. J., Liu, J., Moses, A. J., Horrocks, D. H., and Basak, A. (1996). A two-dimensional single sheet tester incorporating controlled magnetization direction. *Journal of Applied Physisc*, 79(8):4753. doi: 10.1063/1.361661.

de la Barriere, O., Appino, C., Ragusa, C., Fiorillo, F., LoBue, M., and Mazaleyrat, F. (2018). 1-D and 2-D Loss-Measuring Methods: Optimized Setup Design, Advanced Testing, and Results. *IEEE Transactions on Magnetics*, 54(9):1–15. doi: 10.1109/TMAG.2018.2846619.

De Wulf, M., Makaveev, D., Houbaert, Y., and Melkebeek, J. (2003). Design and calibration aspects of small size single sheet testers. *Journal of Magnetism and Magnetic Materials*, 254-255:70–72. doi: 10.1016/S0304-8853(02)00756-4.

Dular, P., Geuzaine, C., Henrotte, F., and Legros, W. (1998). A general environment for the treatment of discrete problems and its application to the finite element method. *IEEE Transactions on Magnetics*, 34(5):3395–3398. doi: 10.1109/20.717799.

Enokizono, M., Suzuki, T., Sievert, J., and Xu, J. (1990). Rotational power loss of silicon steel sheet. *IEEE Transactions on Magnetics*, 26(5):2562–2564. doi: 10.1109/20.104798.

Enokizono, M., Todaka, T., Sashikata, T., Sievert, J., and Ahlers, H. (1992). Magnetic field analysis of rotational loss tester with vertical yoke. *Journal of Magnetism and Magnetic Materials*, 112(1-3):81–84. doi: 10.1016/0304-8853(92)91118-D.

Fonteyn, K. and Belahcen, A. (2008). Numerical and experimental results from a vertical yoke system for measuring magnetic properties of Fe-Si steel sheets. *International Conference on Electrical Machines and Systems (ICEMS)*, pages 434–438.

Geuzaine, C. and Remacle, J.-F. (2009). Gmsh: A 3-D finite element mesh generator with built-in pre- and post-processing facilities. *International Journal for Numerical Methods in Engineering*, 79(11):1309–1331. doi: 10.1002/nme.2579.

Hasenzagl, A., Weiser, B., and Pfützner, H. (1996). Novel 3-phase excited single sheet tester for rotational magnetization. *Journal of Magnetism and Magnetic Materials*, 160:180–182. doi:10.1016/0304-8853(96)00158-8.

Leite, J. V., Benabou, A., da Silva, P., Sadowski, N., Henneron, T., Clénet, S., Kuo-Peng, P., Piriou, F., and Batistela, N. J. (2007). Analysis of a rotational single sheet tester using 3D finite element model taking into account hysteresis effect. *COMPEL - The international journal for computation and mathematics in electrical and electronic engineering*, 26(4):1037–1048. doi: 10.1108/03321640710756366.

Li, A., Li, Y., Zhang, C., Yang, Q., and Zhu, J. (2017). Design of a novel high frequency 2-D magnetic tester with nanocrystalline material. In *International Conference on Electrical Machines and Systems (ICEMS)*, pages 1–5. doi: 10.1109/ICEMS.2017.8056410.

Maeda, Y., Shimoji, H., Todaka, T., and Enokizono, M. (2008). Study of the Counterclockwise/Clockwise (CCW/CW) Rotational Losses Measured with a Two-dimensional Vector Magnetic Property Measurement System. *IEEJ Transactions on Electrical and Electronic Engineering*, 3(2):222–228. doi: 10.1002/tee.20258.

Makaveev, D., von Rauch, M., De Wulf, M., and Melkebeek, J. (2000). Accurate field strength measurement in rotational single sheet testers. *Journal of Magnetism and Magnetic Materials*, 215-216:673–676. doi: 10.1016/S0304-8853(00)00255-9.

Miyagi, D., Yamazaki, T., Otome, D., Nakano, M., and Takahashi, N. (2009). Development of Measurement System of Magnetic Properties at High Flux Density Using Novel Single-Sheet Tester. *IEEE Transactions on Magnetics*, 45(10):3889–3892. doi: 10.1109/TMAG.2009.2022332.

Nencib, N., Kedous-Lebouc, A., and Cornut, B. (1994). 3D analysis of a rotational loss tester with vertical yokes. *Journal of Magnetism and Magnetic Materials*, 133(1-3):553–556. doi: 10.1016/0304-8853(94)90620-3.

Nencib, N., Kedous-Lebouc, A., and Cornut, B. (1995). 2D analysis of rotational loss tester. *IEEE Transactions on Magnetics*, 31(6):3388–3390. doi: 10.1109/20.490391.

Nencib, N., Kedous-Lebouc, A., and Cornut, B. (1996a). Experimental analysis of the field distribution in a large RSST. *Journal of Magnetism and Magnetic Materials*, 160:171–173. doi: 10.1016/0304-8853(96)00147-3.

Nencib, N., Kedous-Lebouc, A., and Cornut, B. (1996b). Performance evaluation of a large rotational single sheet tester. *Journal of Magnetism and Magnetic Materials*, 160:174–176. doi: 10.1016/0304-8853(96)00148-5.

Qiu, F., Ren, W., Tian, G. Y., and Gao, B. (2017). Characterization of applied tensile stress using domain wall dynamic behavior of grain-oriented electrical steel. *Journal of Magnetism and Magnetic Materials*, 432:250–259. doi 10.1016/j.jmmm.2017.01.076.

Salz, W. (1994). A two-dimensional measuring equipment for electrical steel. *IEEE Transactions on Magnetics*, 30(3):1253–1257. doi: 10.1109/20.297761.

Sievert, J. (2011). Two-dimensional magnetic measurements - history and achievements of the workshop. *Przeglad Elektrotechniczny*, 87(9b):2–10.

Sievert, J., Ahlers, H., Enokizono, M., Kauke, S., Rahf, L., and Xu, J. (1992). The measurement of rotational power loss in electrical sheet steel using a vertical yoke system. *Journal of Magnetism and Magnetic Materials*, 112(1-3):91–94. doi: 10.1016/0304-8853(92)91121-9.

Sievert, J., Shinji, S., Hiroyasu, S., Takashi, T., Enokizono, M., and Yoshitaka, M. (2007). Study of the counterclockwise/clockwise (CCW/CW) rotation problem with the measurement of 2-dimensional magnetic properties. *Przeglad Elektrotechniczny*, 83(4):18–24.

Tumanski, S. (2005). New design of the magnetising circuit for 2D-testing of electrical steel. *Przeglad Elektrotechniczny*, 81(5):32–34.

Tumanski, S. (2011). *Handbook of Magnetic Measurements*. CRC Press, 1st edition.

Tumanski, S. and Bakon, T. (2001). Measuring system for two-dimensional testing of electrical steel. *Journal of Magnetism and Magnetic Materials*, 223(3):315–325. doi: 10.1016/S0304-8853(00)01332-9.

Walpole, L. (1985). Evaluation of the elastic moduli of a transversely isotropic aggregate of cubic crystals. *Journal of the Mechanics and Physics of Solids*, 33(6):623–636. doi 10.1016/0022-5096(85)90006-7.

Wanjiku, J. and Pillay, P. (2015). Design Considerations of 2-D Magnetizers for High Flux Density Measurements. *IEEE Transactions on Industry Applications*, 51(5):3629–3638. doi: 10.1109/TIA.2015.2417834.

Wanjiku, J. and Pillay, P. (2016). Design of a Sinusoidally Wound 2-D Rotational Core Loss Setup With the Consideration of Sensor Sizing. *IEEE Transactions on Industry Applications*, 52(4):3022–3032. doi: 10.1109/TIA.2016.2551683.

Yue, S., Li, Y., Yang, Q., Zhang, K., and Zhang, C. (2019a). Comprehensive Investigation of Magnetic Properties for Fe-Si Steel Under Alternating and Rotational Magnetizations Up to Kilohertz Range. *IEEE Transactions on Magnetics*, 55(7):1–5. doi: 10.1109/TMAG.2019.2895152.

Yue, S., Li, Y., Zhang, C., and Yang, Q. (2019b). Considerations of the Magnetic Field Uniformity for 2-D Rotational Core Loss Measurement. In *Proceedings of Energy Conversion Congress and Exposition (ECCE)*, pages 901–907, Baltimore. doi: 10.1109/ECCE.2019.8913047.

Zhu, J. and Ramsden, V. (1993). Two dimensional measurement of magnetic field and core loss using a square specimen tester. *IEEE Transactions on Magnetics*, 29(6):2995–2997. doi: 10.1109/20.281098.

Zouzou, S., Kedous-Lebouc, A., and Brissonneau, P. (1992). Magnetic properties under unidirectional and rotational field. *Journal of Magnetism and Magnetic Materials*, 112(1-3):106–108. doi: 10.1016/0304-8853(92)91125-D.

Zurek, S. (2017). *Characterisation of Soft Magnetic Materials Under Rotational Magnetisation*. CRC Press, Boca Raton, 1 edition. doi:10.1201/b22374.